Supporting Information

Poly(polyoxometalate)s: Assembled by {Ni_6PW_9} Units: From Ring-shaped Ni_{24}-Tetramer to Rod-shaped Ni_{40}-Octamer

Ling Huang,[a] Jie Zhang,[a] Lin Cheng,[a] and Guo-Yu Yang[a,b]*

[a]*State Key Laboratory of Structural Chemistry, Fujian Institute of Research on the Structure of Matter, Chinese Academy of Sciences, Fuzhou, Fujian 350002, China. E-mail: ygy@fjirsm.ac.cn*

[b]*School of Chemistry, Bejing Institute of Technology, Beijing 100081, China. E-mail: ygy@bit.edu.cn*

Experimental Section

All chemicals employed in this study were analytical reagent. Elemental analyses of C, H and N were carried out with a Vario EL III elemental analyzer. IR spectra (KBr pellets) were recorded on an ABB Bomen MB 102 spectrometer. Thermal analyses were performed in a dynamic oxygen atmosphere with a heating rate of 10 ºC/min using a METTLER TGA/SDTA 851^e thermal analyzer. X-ray diffraction data were collected on a Mercury-CCD diffractometer with graphite-monochromated MoK_α (λ = 0.71073 Å) at room temperature. The program SADABS was used for the absorption correction. The structures were solved by the direct method and refined on F^2 by full-matrix least-squares methods using the SHELX97 program package. Powder XRD patterns were obtained using a Philips X'Pert-MPD diffractometer with CuK_α radiation (λ = 1.54056 Å). Variable temperature susceptibility measurements were carried out in the temperature range 2-300 K at a magnetic field of 1 kOe for **1** and **2** on polycrystalline samples with a Quantum Design MPMS XL-5 SQUID magnetometer. All the magnetic susceptibility data were corrected for magnetization of the sample holder and for diamagnetic contribution estimated from Pascal's constants.

Synthesis:

Synthesis of **1** and **2**: $Na_9[A\text{-}\alpha\text{-}PW_9O_{34}]\cdot nH_2O$ were prepared by a literature method.[1] A sample of PW_9 (0.24 g) and $Ni(OAc)_2\cdot 4H_2O$ (0.20 g) were stirred in distilled water (8 mL), and then enMe (0.20 mL for **1**) or en (0.10 mL for **2**) and acetic acid (0.12 mL for **1**, and 0.10 mL for **2**) were dropwise added with continuous stirring for 20 min (pH_s = 6.2 for **1** and 5.7 for **2**). The resulting solution was sealed in a 35-mL stainless steel reactor with a Teflon liner and heated at 170 °C for 3 days and then cooled to room temperature (pH_e= 6.0 for **1** and 5.6 for **2**). Green prismatic crystals of **1** and **2** were obtained (note the B type isomers were obtained from the A type starting material). Yields: 27% for **1** and 30% for **2** based on $Ni(OAc)_2\cdot 4H_2O$, respectively. Details of elemental analysis, IR, XRD, TGA, and magnetic measurements of 1 and 2 are given under below.

1 A. P. Ginsberg, *Inorganic Syntheses*, Vol. **27**, Wiely, New York, 1990, p.85.

Crystal data:

Crystal data: **1**: Mr = 12262.69, monoclinic, $P2_1/n$, a = 20.518(3), b = 23.518 (3), c = 27.721(5) Å, β = 111.402(2)º, V = 12454(3) Å^3, Z = 2, ρ_{calcd} = 3.270 g cm^{-3}, μ = 18.509 mm^{-1}, F(000) = 11108, GOF = 1.126. A total of 107016 reflections were collected, 28481 of which were unique (R_{int}= 0.0822). R_1/wR_2 = 0.0863/0.1896 for 1397 parameters and 26117 reflections ($I > 2\sigma(I)$). **2**: Mr = 23793.07, triclinic, P-1, a = 13.724(3), b = 28.811(8), c = 30.191(8) Å, α = 108.865(4)º, β = 90.168(2)(5)º, γ = 97.909(2)º, V = 11174(5) Å^3, Z = 1, ρ_{calcd} = 3.536 g·cm^{-3}, μ = 20.967 mm^{-1}, F(000) = 10664, GOF = 1.031. A total of 132870 reflections were collected, 50914 of which were unique (R_{int}= 0.1043). R_1/wR_2 = 0.0904/0.1922 for 2455 parameters and 29013 reflections ($I > 2\sigma(I)$). CCDC-821914-821915 contains the supplementary crystallographic data for this paper. These data can be obtained free of charge from The Cambridge Crystallographic Data Centre via www.ccdc.cam.ac.uk/data_request/cif.

Elemental analysis and IR data:

Elemental analysis calcd (%) for $[Ni(enMe)_2][H_2Ni_{24}P_4W_{36}(OH)_{12}O_{136}(enMe)_{12}(OAc)_4(H_2O)_{12}]\cdot 10H_2O$ ($[Ni(enMe)_2]\cdot$**1**$\cdot 10H_2O$) and $[Ni(en)_2]_2[Ni(en)_2(H_2O)_2]_2[Ni(en)(H_2O)_2]_2[H_4Ni_{40}P_8W_{72}(OH)_{18}O_{272}(en)_{18}(OAc)_2(WO_4)_2(H_2O)_{18}]\cdot 10H_2O$ ($[Ni(en)_2]_2[Ni(en)_2(H_2O)_2]_2[Ni(en)(H_2O)_2]_2\cdot$**2**$\cdot 10H_2O$) (OAc = CH3COO-; enMe = 1,2-diaminopropane; en = ethylenediamine) are as follows:

(1) $\mathbf{C_{50}H_{210}N_{28}Ni_{25}O_{178}P_4W_{36}}$ (**1**, M_r = 12262.69): C 4.90, H 1.73, N 3.20, found: C 5.52, H 1.90, N 3.46. IR (KBr, cm^{-1}): 3433s, 3169s, 1617m, 1556m, 1400s, 1199m, 1041s, 942s, 848m, 786m, 708m, 584m, 410w.

(2) $\mathbf{C_{60}H_{324}N_{56}Ni_{46}O_{338}P_8W_{74}}$ (**2**, M_r = 23793.07): C 3.03, H 1.37, N 3.30, found: C 3.47, H 1.66, N 3.64. IR (KBr, cm^{-1}): 3433s, 3144s, 1614s, 1454w, 1400s, 1236w, 1281w, 1038s, 941m, 899w, 842, 778w, 770m, 591w, 504w.

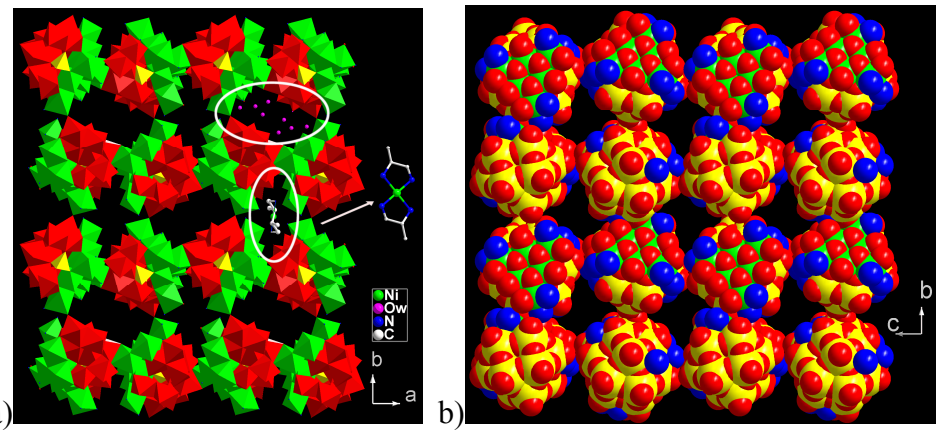

Figure S1. a) View of the stacking mode of **1** along the *c*-axis, showing the –ABAB…– arrangement and the location of the $[Ni(enMe)_2]^{2+}$ complexes and the lattice water molecules. b) View of the space filling of **1** along the *a*-axis, showing the –ABAB…– arrangement, in which the $[Ni(enMe)_2]^{2+}$ complexes and the lattice water molecules are omitted for clarity.

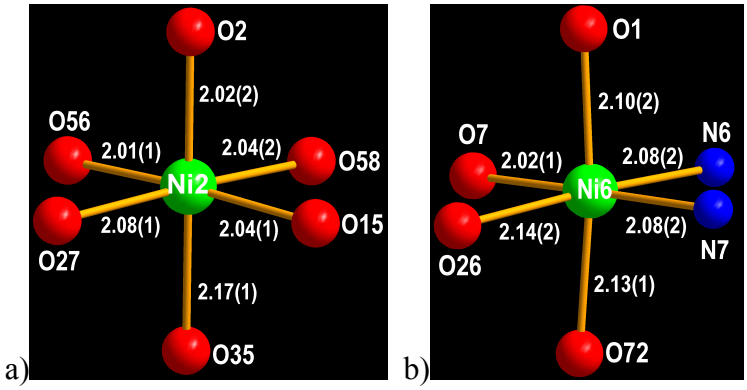

Figure S2. The ball-and-stick representations of Ni2- and Ni6-based octahedra with the square plane Ni-O bond lengths and the axial Ni-O bond lengths in **1**, respectively.

As shown in Figure S2, the square plane Ni-O 2.01(1)~2.08(1) Å and the axial Ni-O 2.02(2)~**2.17**(1) Å in **Ni2**O_4**O2O35** octahedron (Figure S2a), while in **Ni6**O_4**O1O72** octahedron (Figure S2b), the square plane Ni-O 2.02(1)~2.14(2) and the axial Ni-O **2.10**(2)~**2.13**(1)Å respectively, in which the lengths of the axial Ni-O bonds (**Ni2-O35**, **Ni6-O72** and **Ni6-O1**) are longer than that of the square plane Ni-O bonds, showing the John-Teller distortion with the axial elongation exists in these Ni-octahedra. Such the axial elongation of the octahedra reduces or overcomes large steric hindrance to some extent when the big **1b** unit attacks **1a** unit, and favors to the occurrence of the substitution reaction between **1a** and **1b** units, resulting in a novel circular poly(POT) tetramer.

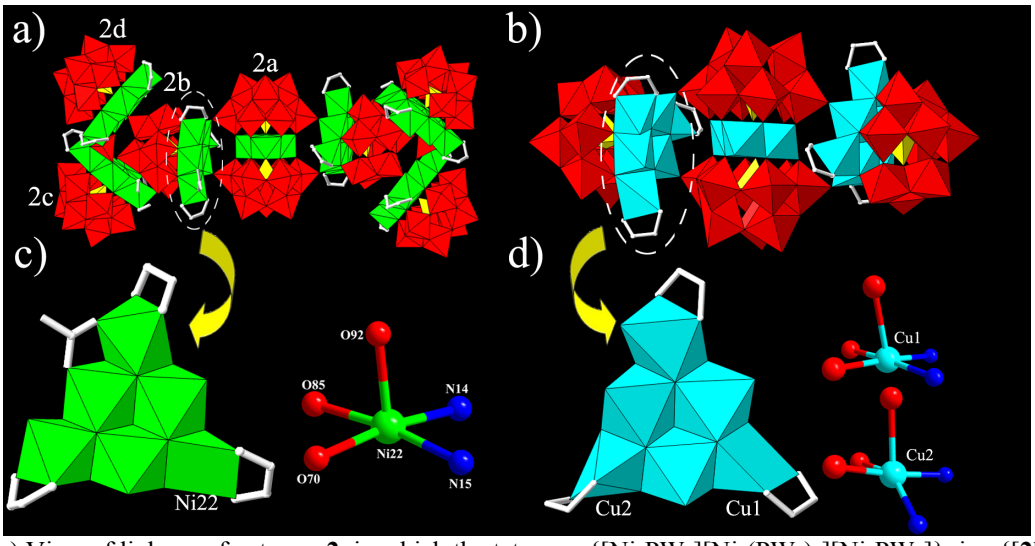

Figure S3. a) View of linkage of octamer **2**, in which the tetramer $\{[Ni_6PW_9][Ni_4(PW_9)_2][Ni_6PW_9]\}$, i.e. {[**2b**][**2a**][**2b**]}, is included. b) View of linkage of Cu_{16}-based tetramer $\{[Cu_6PW_9][Cu_4(PW_9)_2][Cu_6PW_9]\}$. c) The $\{Ni_6\}$ unit containing a penta-coordinated **Ni22** center with square pyramid geometry in **2b** and the coordination environment of penta-coordinated **Ni22** in **2b**. d) The $\{Cu_6\}$ unit in Cu_{16}-based tetramer and the coordination environment of penta-coordinated Cu1 and Cu2 centers with square pyramid and trigonal bipyramid, respectively**.**

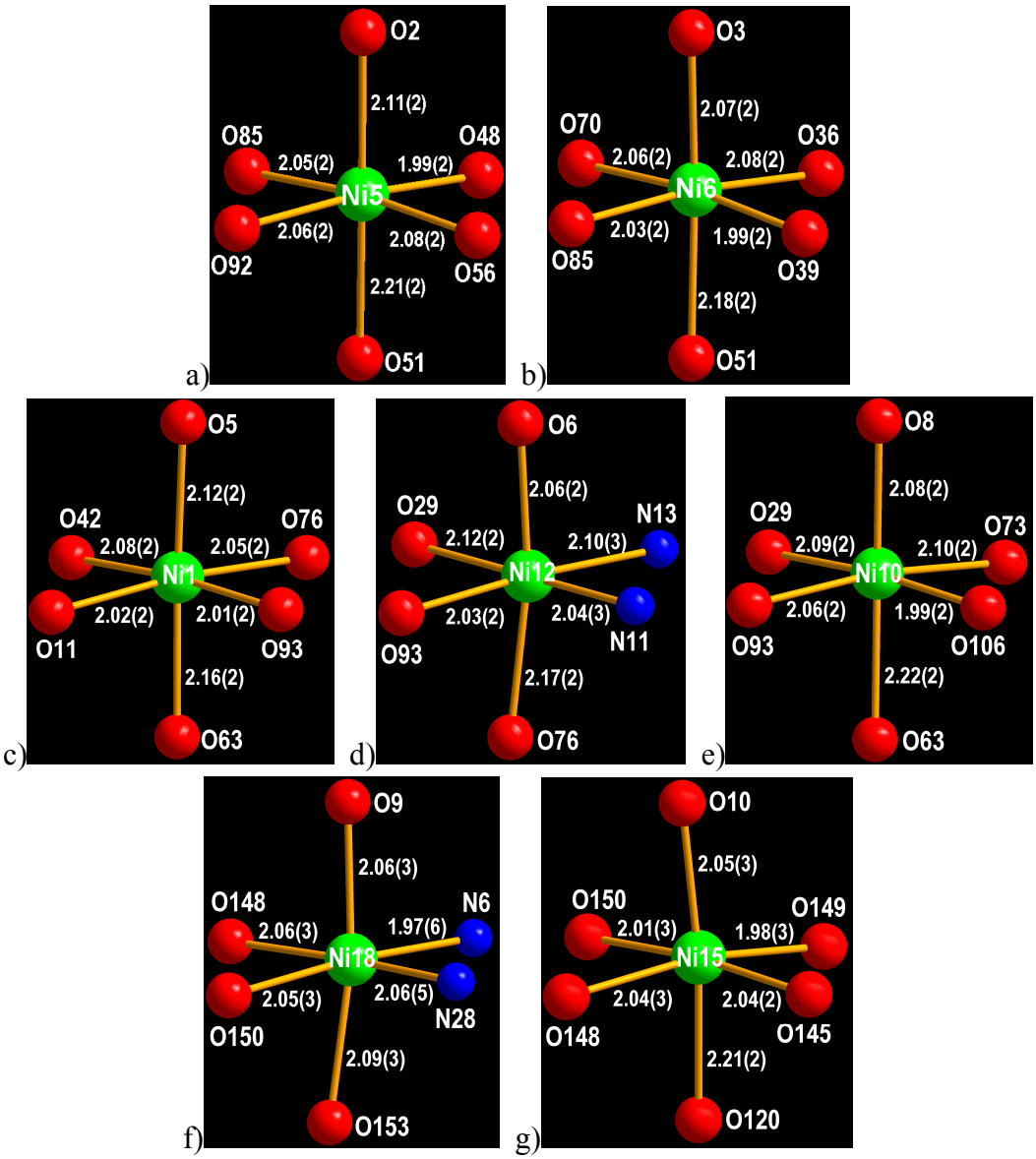

Figure S4. a~g) The ball-and-stick representations of Ni5-/Ni6-/Ni1-/Ni12-/Ni10-/Ni18-/Ni15-based octahedra with the square plane Ni-O bond lengths and the axial Ni-O bond lengths in **2**, respectively.

As shown in Figure S4a/b, the square plane Ni-O 1.99(2)~2.08(2) Å and the axial Ni-O 2.11(2)~2.21(2) Å in **Ni5**O_4**O2O51** octahedron (Figure S4a), while in **Ni6**O_4**O3O51** octahedron (Figure S4b), the square plane Ni-O 1.99(2)~2.08(2) and the axial Ni-O 2.07(2)~2.18(2)Å respectively, in which the lengths of the axial Ni-O bonds (Ni5-O2, Ni5-O51, Ni6-O3 and Ni6-O51) are longer than that of the square plane Ni-O bonds, showing the John-Teller distortion with the axial elongation exists in these Ni-octahedra. Such the axial elongation of the octahedra in combination of the penta-coordinated **Ni22**-based square pyramid **Ni22**O_3N_2 (Figure S3c) with less steric hinderance will reduce or overcome large steric hindrance when the big **2a** unit attacks two **2b** units. These two factors favor to the occurrence of the substitution reaction between **2a** and two **2b** units to some extent and the formation of the poly(POT) tetramer {[**2b**][**2a**][**2b**]}, which can be viewed as the synergistic effect between the square pyramids with the less steric hinderance and the Jahn-Teller effect of the octahedra with the axial elongation.

The detailed bond lengths in **Ni(1,10,12,15,18)**-based octahedra containing **O(5**,**6**,**8,9,10)** atoms are list as follows: 1) In **Ni1**O_4**O5O63** octahedron (Figure S4c), the square plane Ni-O 2.01(2)~2.08(2) Å, and the axial Ni-O 2.12(2)~2.16(2)Å; 2) in **Ni12**O_2N_2**O6O76** octahedron (Figure S4d), the square plane Ni-N/O 2.03(2)~2.12(2) Å, and the axial Ni-O 2.06(2)~2.17(2) Å; 3) in **Ni10**O_4**O8O63** octahedron (Figure S4e), the square plane Ni-O 1.99(2)~2.10(2) Å, and the axial Ni-O 2.08(2)~2.22(2) Å; 4) in **Ni18**O_2N_2**O9O153** (Figure S4f), the square plane Ni-N/O 1.97(2)~2.06(2) Å, and the axial Ni-O 2.06(2)~2.09(3) Å; 5) in **Ni15**O_4**O10O120** (Figure S4g), the square plane Ni-O 1.98(3)~2.04(2) Å, and the axial Ni-O 2.05(3)~2.21(2) Å. By comparing the bond length regions of the above five Ni-based octahedra containing **O(5**,**6**,**8,9,10)** atoms and found that all the axial Ni-O lengths are longer than the square plane Ni-O lengths, indicating Jahn-Teller effect with the axial elongation exists in the above five Ni-octahedra, which reduces or overcomes large steric hindrance when the substitution reactions take place, and favor to the formation of the hexamer {[**2c**][**2b**][**2a**][**2b**][**2c**]} and the octamer **2**. Here, the driving force of the assembly of the hexamer {[**2c**][**2b**][**2a**][**2b**][**2c**]} and the octamer **2** is mainly attributed to the Jahn-Teller effect of the octahedra with the axial elongation.

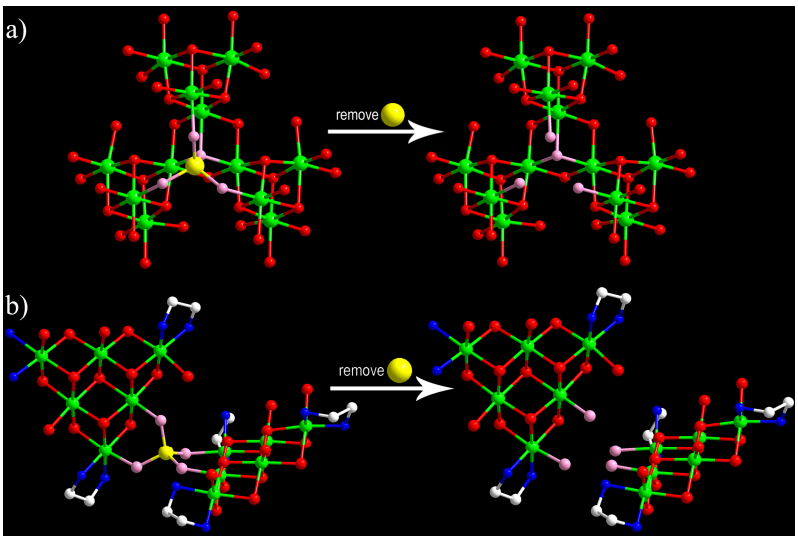

Figure S5. a) The ball-and-stick view of $\{WNi_{12}\}$ trimer in cluster $[Ni_{12}(OH)_9WO_4(W_7O_{26}(OH))(PW_9O_{34})_3]^{25-}$ (**3**) and the $\{Ni_{12}\}$ trimer after the removing of the central W atom. b) The ball-and-stick view of $\{WNi_{12}\}$ dimer in octamer **2** and the two isolated Ni_6 clusters formed after the removing of the central W atom Color code: W, yellow; the O atoms linked to the W atom and Ni atoms, pink; the O atoms only bonded to the Ni atoms, red; the Ni atoms, green.

As shown in Figure S5, the role of the WO_4 group in **2** and **3** are different. Four O atoms of WO_4 group of $\{WNi_{12}\}$ trimer in **3** link the Ni_{12} unit via three μ-O from three Ni_4 cores and a μ_4-O atom shared by one W and three Ni_4 cores (Figure S5a, left). If the W atom is removed from the $\{WNi_{12}\}$ trimer in **3**, three μ-O and one μ_4-O atoms will become three terminal O and one μ_3-O linked three Ni_4 cores (Figure S5a, right), respectively, i.e. three Ni_4 cores in the $\{Ni_{12}\}$ trimer (Figure S5a, right) still connect each other by a μ_3-O atom, even if the absence of the W atom. Two of three Ni_4 cores in $\{Ni_{12}\}$ trimer link each other not only by a μ-O atom but also by a μ_3-O atom (Figure S5a, right). Therefore, the W atom is not necessary in the formation of the $\{Ni_{12}\}$ trimer in **3**. In octamer **2**, four O atoms of the WO_4 unit in the dimer $\{WNi_{12}\}$ (Figure S5b, left) connect two **Ni_6** clusters via four μ-O atoms. If the W atom is removed from the dimer $\{WNi_{12}\}$ in **2**, not only four μ-O atoms will become terminal water ligands but also the linkages between two **Ni_6** clusters will be cut (Figure S5b, right). Therefore, the W atoms as inorganic bridges are necessary and plays a crucial role in the formation of the dimer $\{WNi_{12}\}$ and **2**, and such linking mode is first observed in TM-substituted poly(POM) chemistry.

So, the difference between **2** and **3** can be concluded as: 1) Four O atoms of the WO_4 group in **3** link to the Ni_{12} unit via three μ-O of three Ni_4 cores and a μ_4-O atom shared by one W and three Ni_4 cores. If the W atom is removed from **3**, three μ-O and one μ_4-O atoms will become three terminal O and one μ_3-O linked three Ni_4 cores, respectively, i.e. three Ni_4 cores still connect each other by a μ_3-O atom, even if the absence of the W atom. Two of three Ni_4 cores in **3** link each other not only by a μ-O atom but also by a μ_3-O atom. Therefore, the W atom is not necessary in the formation of **3**. 2) In **2**, four O atoms of the WO_4 unit connect two adjacent **Ni_6** clusters via four μ-O atoms. If the W atom is removed from **2**, not only four μ-O atoms will become terminal water ligands but also the linkages between two adjacent **Ni_6** clusters will be cut.

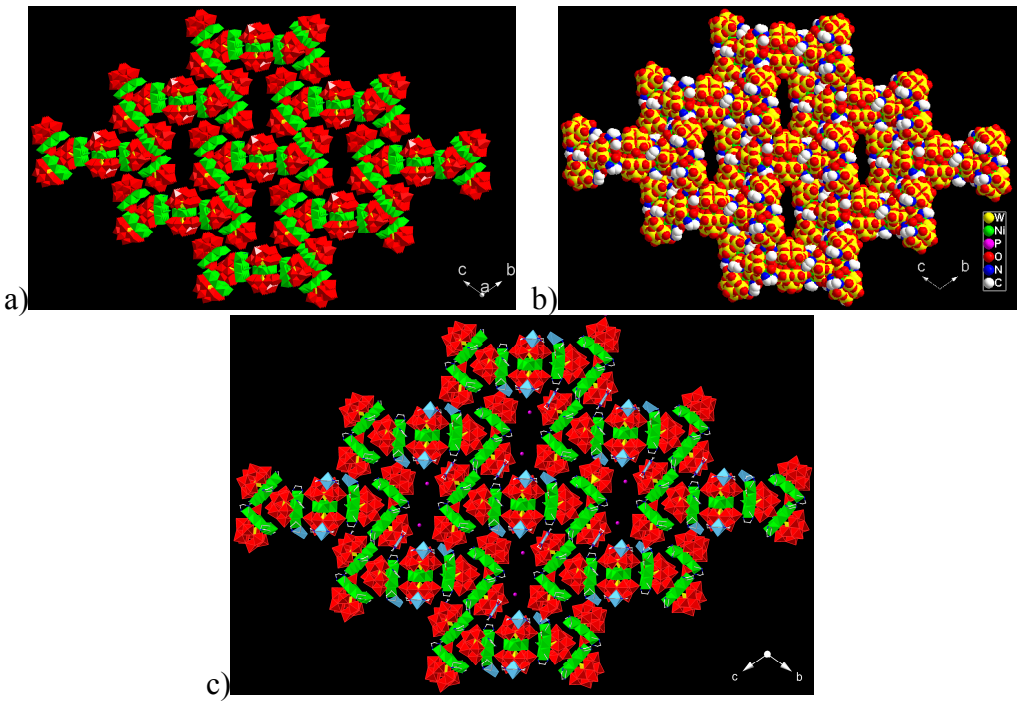

Figure S6. a) and b)The stacking mode and space filling of octamer **2** along the *a*-axis, respectively. The Ni-based complexes and lattice water molecules are omitted foe clarity. c) The stacking mode of octamer **2** along the *a*-axis, showing the location of the Ni-based complexes and lattice water molecules. Notice that only the lattice water molecules located in the large channels of **2**. Violet ball: H_2O; cyan Ni-based polyhedra.

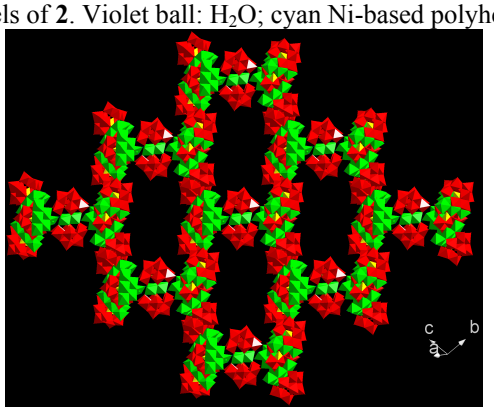

Figure S7. View of the extra large channels in **2** along the rotated *a*-axis.

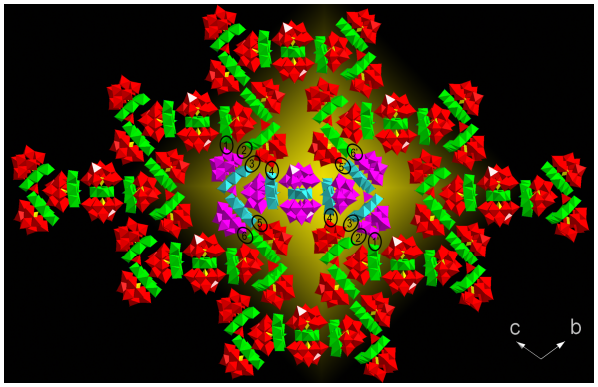

Figure S8. The stacking mode of the octamer **2** in the structure along the a-axis, in which the central octamer **2** is marked different color for distinguishing the around eight octamers **2**. Color code: Violet for $\mathbf{PW_9}$ units and WO_4 groups, and cyan for $\mathbf{Ni_6}$ units in the central octamer; while red for $\mathbf{PW_9}$ units and WO_4 groups, and green for $\mathbf{Ni_6}$ units in the around eight octamers **2**.

To compound **2**, in which some water ligands of the $\mathbf{Ni_6}$ units are very good centers for further structural derivation through intermolecular substitution reactions i.e. by replacing the related water ligand of the $\mathbf{Ni_6}$ units with the adjacent terminal O atoms of the PW_9 units via the Ni-O=W linkages when the steric hindrance is allowable under the rational conditions, which provide the potential for making extended poly(POT)s or real open frameworks with large or extra-large channels built up from the big SBUs of octamer **2.**

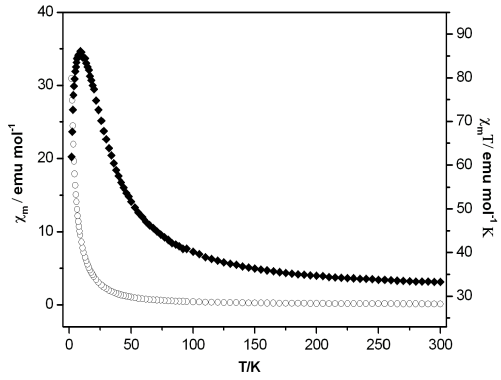

Figure S9. Temperature dependence of $\chi_m T$ (◆) and χ_m (○) values for **1** between 2.0 to 300 K.

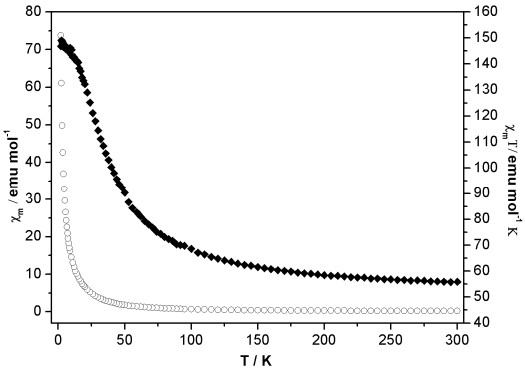

Figure S10. Temperature dependence of $\chi_m T$ (◆) and χ_m (○) values for **2** between 2.0 to 300 K.

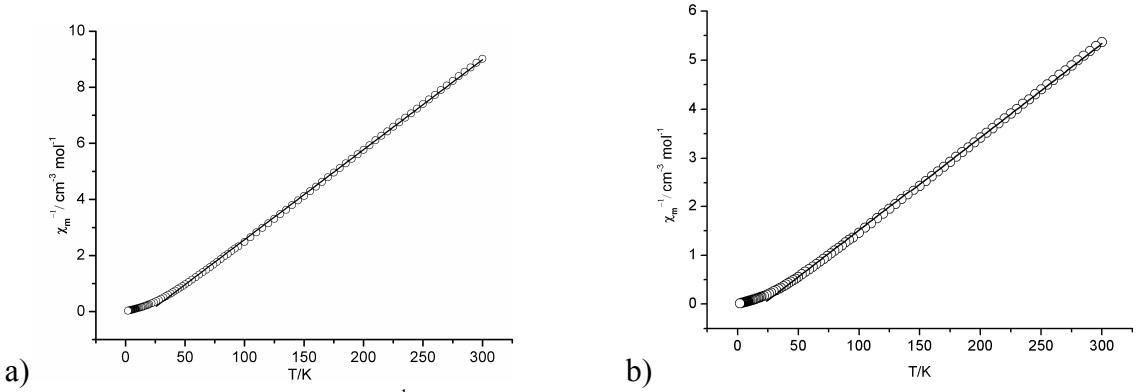

Figure S11. Temperature dependence of χ_m^{-1} for **1** and **2**. The solid lines are the best-fit according to the Curve-Weiss law.

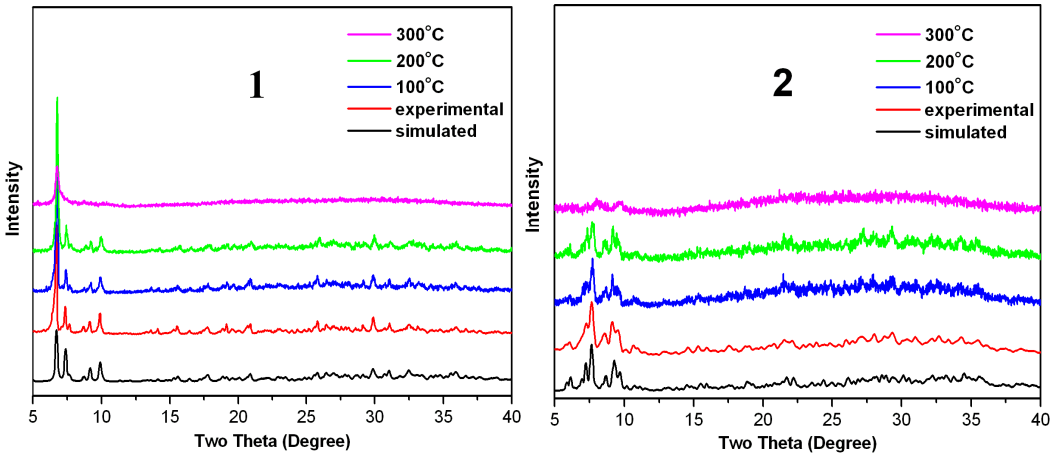

Figure S12. Thermodiffractograms of poly(POT)s samples **1** and **2,** showing the bulk product are in good agreement with the calculated patterns based on the results from single-crystal X-ray diffraction. Crystals of **1** and **2** are stable lower than 300°C.

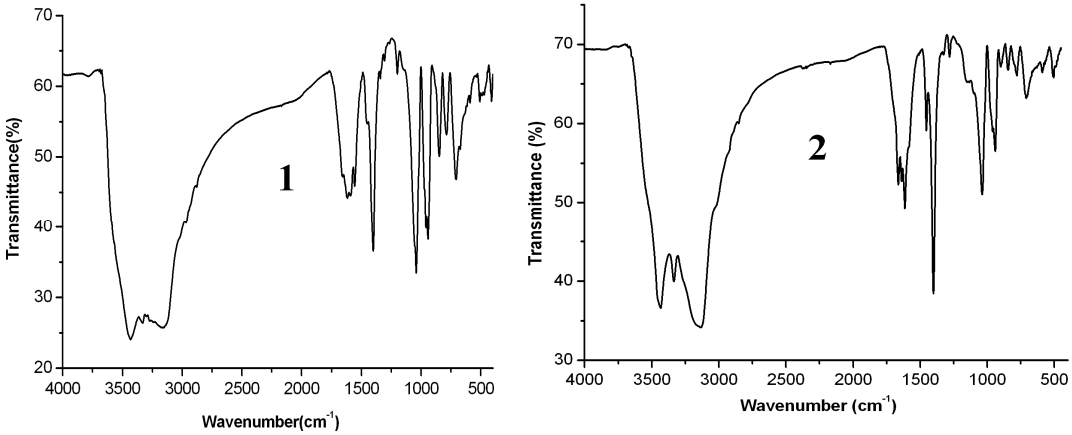

Figure S13. IR spectra of poly(POT)s **1** and **2,** exhibiting an intense band at 1040 cm^{-1}, attributed to the feature of $\nu_{P\text{-}O}$, and bands at 940 cm^{-1} due to $\nu_{W=O}$, bands at 850, 790, and 710 cm^{-1} due to $\nu_{M\text{-}O\text{-}M}$ (M = W or Ni). The characteristics of the $-NH_2$ and $-CH_2$ groups are fallen in the 1400 and 3100-3300 cm^{-1} region.

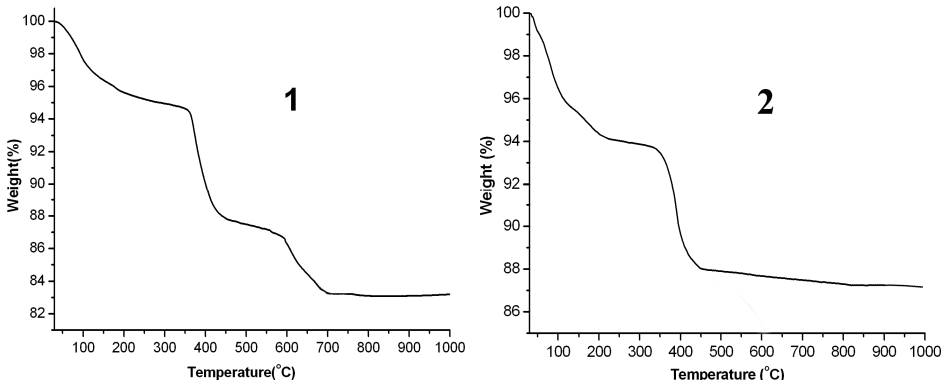

Figure S14. TG curves of poly(POT)s **1** and **2**, respectively**.**

As shown in Figure S13, the TG curve of **1** shows three major weight loss stages in the regions about 30-351, 351-574, and 574-700°C, while the TG curve of **2** exhibits two steps weight loss stages in the regions about 30-318 and 318-800°C, respectively. To tetramer **1**, the observed total weight loss of **1** (16.9%) is in agreement with the calculated value of **1** (15.5%). The first weight loss of **1** is 5.4% from 30~351°C, assigned to the release of 10 lattice water molecules, 12 coordinated water ligands and the partial enMe ligands (three enMe, calcd 5.0%), followed by the loss of 7.8% from 351-574 °C corresponding to the removal of the remanent enMe ligands (eleven enMe, calcd 6.6%), the third weight loss of 3.7% between 574-700 °C corresponding to the removal of four carboxyl groups and the dehydration of the protons and the hydroxyl groups (calcd 3.9%). To octamer **2**, the observed total weight loss of **2** (12.8%) is in agreement with the calculated value of **2** (11.9%). The first weight loss is 6.2% from 30-318 °C, assigned to the release of 10 lattice water molecules, 26 coordinated water ligands and the partial en ligands (fourteen en, calcd 6.3%), followed by the loss of 6.6% from 318-800 °C corresponding to the removal of the remanent en ligands (fourteen en ligands) and two carboxyl groups, as well as the dehydration of the protons and the hydroxyl groups (calcd 5.6%).